J. Fluid Mech. (2017), *vol.* 811, *pp.* 525–543. © Cambridge University Press 2016
doi:10.1017/jfm.2016.763

Effects of inertia and turbulence on rheological measurements of neutrally buoyant suspensions

Esperanza Linares-Guerrero[1], Melany L. Hunt[1,†] and Roberto Zenit[2]

[1]Division of Engineering and Applied Science, California Institute of Technology, Pasadena, CA 91125, USA

[2]Instituto de Investigaciones en Materiales, Universidad Nacional Autónoma de México, Apdo. Postal 70-360, México D.F. 04510, México

(Received 20 November 2015; revised 20 July 2016; accepted 9 November 2016; first published online 13 December 2016)

For low-Reynolds-number shear flows of neutrally buoyant suspensions, the shear stress is often modelled using an effective viscosity that depends only on the solid fraction. As the Reynolds number (Re) is increased and inertia becomes important, the effective viscosity also depends on the Reynolds number itself. The current experiments measure the torque for flows of neutrally buoyant particles in a coaxial-cylinder rheometer for solid fractions, ϕ, from 10 % to 50 % and Reynolds numbers based on particle diameter from 2 to 1000. For experiments for Reynolds of $O(10)$ and solid fractions less than 30 %, the effective viscosity increases with Reynolds number, in good agreement with recent numerical simulations found in the literature. At higher solid fractions over the same range of Re, the results show a decrease in torque with shear rate. For Reynolds numbers greater than 100 and lower solids concentrations, the effective viscosity continues to increase with Reynolds number. However, based on comparisons with pure fluid measurements the increase in the measured effective viscosity results from the transition to turbulence. The particles augment the turbulence by increasing the magnitude of the measured torques and causing the flow to transition at lower Reynolds numbers. For the highest solid fractions, the measurements show a significant increase in the magnitude of the torques, but the effective viscosity is independent of Reynolds number.

Key words: particle/fluid flows, suspensions, transition to turbulence

1. Introduction

There is an extensive body of work on the rheology of neutrally buoyant suspensions (Batchelor 1970; Larson 1998; Foss & Brady 2000; Stickel & Powell 2005). Typically, these studies investigate suspensions in which the Reynolds number is small, $Re \ll 1$, where Re is defined as $Re = \rho\dot{\gamma}d^2/\mu$, ρ is the fluid density, $\dot{\gamma}$ is the shear rate, d is the particle diameter and μ is the fluid viscosity. For low-Reynolds-number suspensions, the shear stress, τ, is assumed to depend linearly on $\dot{\gamma}$ and an effective viscosity, μ'; hence, $\tau = \mu'\dot{\gamma}$. In this regime, the effective viscosity depends only on the solid fraction, ϕ, and can be estimated through various

†Email address for correspondence: hunt@caltech.edu

Downloaded from https://www.cambridge.org/core. Universidad Nacional de Mexico (UNAM), on 26 Apr 2018 at 19:08:51, subject to the Cambridge Core terms of use, available at https://www.cambridge.org/core/terms. https://doi.org/10.1017/jfm.2016.763

Downloaded from https://www.cambridge.org/core. Universidad Nacional de Mexico (UNAM), on 26 Apr 2018 at 19:08:51, subject to the Cambridge Core terms of use, available at https://www.cambridge.org/core/terms. https://doi.org/10.1017/jfm.2016.763

semi-empirical relations, such as the Eilers or Krieger–Dougherty relations. For solid fractions greater than approximately 40 %, the effective viscosity may also depend on the shear rate (Larson 1998; Foss & Brady 2000; Stickel & Powell 2005; Brown *et al.* 2010).

As the particle Reynolds number increases, both the inertia of the fluid and solid phases become important (Batchelor 1970; Verberg & Koch 2006; Kulkarni & Morris 2008). Recent simulation studies calculate the magnitude of the total stress as a function of the Reynolds number and solid fraction (Kulkarni & Morris 2008; Picano *et al.* 2013; Yeo & Maxey 2013). Kulkarni & Morris (2008) used the lattice-Boltzmann method to calculate the particle contribution to the bulk stress for a suspension in a wall-bounded shear flow. These simulations were performed for particle Reynolds numbers from 0.04 to 16 (note that Kulkarni and Morris defined the Reynolds number based on particle radius rather than the definition used in this paper) and for solid fractions from 0.05 to 0.3. They computed the effective viscosity in two ways: from the shear stress on the bounding walls and from a computation of the volume-averaged stresses within the bulk of the flow. The two methods produced similar results for the lowest solid fractions and showed approximately a 10 % difference at the highest solid fraction because of particle slip at the walls and a lower reduced shear rate in the central region of the flow.

The effective viscosity results of Kulkarni & Morris (2008) are found in figure 1 as a function of solid fraction and Reynolds number. At the lowest solid fractions ($\phi < 0.2$) and Reynolds numbers ($Re < 4$), the dependence of μ' on solid fraction matches the Eilers relation, $\mu' = \mu[(1 + a\phi)/(1 - \phi/\phi_m)]^2$, using $a = 1.5$ and $\phi_m = 0.58$ as assumed by Kulkarni & Morris (2008) (identified as Eilers 1 in figure 1). At $\phi = 0.2$ the effective viscosity shows an increase with Reynolds number with the effective viscosity at $Re = 16$ twenty per cent higher than found at $Re = 0.04$. At $\phi = 0.3$, their simulations showed a slight shear thinning (approximate 6 % drop) for $Re < 0.4$, and an increase of approximately 33 % at $Re = 16$ compared to the values at the $Re = 0.4$. The authors stated that for $\phi = 0.3$, the slight drop in the effective viscosity and then subsequent rise resulted from ordering of the microstructure in the flow direction followed by an increase in the symmetric first moment (Batchelor 1970) for increasing Reynolds numbers. Over the range of conditions considered, the authors found that the contributions from the acceleration and Reynolds stresses were small compared with the contribution from this term (Kulkarni & Morris 2008).

Yeo & Maxey (2013) considered a uniform shear flow rather than a wall-bounded flow. They use a lubrication-corrected, force-coupling method to calculate the stresses and the self-diffusion coefficient for Re from 0.02 to 8 and solid fractions from 0.2 to 0.4. In their simulations, they did not include the Reynolds stresses in the calculation of the effective viscosity. As shown in figure 1, the effective viscosity from their simulations increased as the Reynolds number increased above one; however, at $\phi = 20$ % the effective viscosity is approximately 7 % lower than Kulkarni & Morris (2008) and at $\phi = 30$ % it is 37 % lower in the highest-Reynolds-number studies ($Re = 8$); in their paper, they compared with the Eilers relation using $a = 1.25$ and $\phi_m = 0.63$ (Eilers 2 in figure 1). Although the Reynolds stresses were not included in the calculation, they estimate that the magnitude of such stresses are an order of magnitude smaller than the particle stresses. They also argue that using a pure shear flow, as opposed to the wall-bounded flow used by Kulkarni & Morris (2008), may contribute to the differences in the calculations of μ', especially at higher solid fractions.

Picano *et al.* (2013) also computed the effective viscosity for Reynolds numbers from 0.4 to 40 and solid fractions from 0.11 to 0.31; their results are also found in figure 1. They used an immersed boundary method from Breugem (2012) to

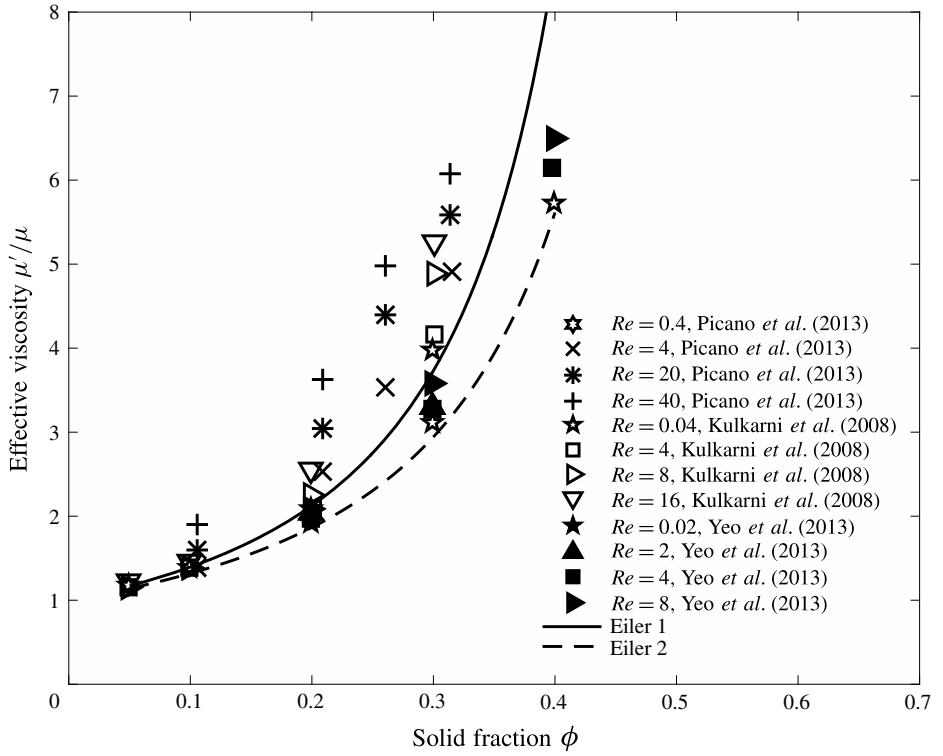

FIGURE 1. Effective viscosity for inertial suspensions as a function of solid fraction from numerical simulations made by Kulkarni & Morris (2008), Picano *et al.* (2013), Yeo & Maxey (2013). Continuous and dashed lines correspond to Eilers relation with $a = 1.5$ and $\phi_m = 0.58$ and $a = 1.25$ and $\phi_m = 0.63$ respectively.

compute the stresses in a wall-bounded suspension, similar to Kulkarni & Morris (2008). Their results are up to 15 % greater than those found by Kulkarni & Morris (2008). Note that to compute the effective viscosity, they used the shear stress at the wall and divided by the average shear rate across the channel; as shown by Kulkarni & Morris (2008) for $\phi = 0.3$, this calculation gives a higher effective viscosity than found by computing the effective viscosity from the particle contribution to the volume-averaged bulk stress within the flow. This same numerical method has recently been used to examine laminar and turbulent flow of a suspension in a channel for a channel Reynolds numbers up to 5000 and in which a particle Reynolds number is greater than 100 (Picano, Breugem & Brandt 2015).

An additional numerical study by Trulsson, Andreotti & Claudin (2012) considered the transition from viscous to *inertial* regime in dense two-dimensional suspensions using a discrete element model coupled to a fluid solver. Their results show a transition from linear to quadratic dependence on the shear rate at volume fractions that are close to the jamming transition. Although the authors use the term 'inertial suspension' they assume a Stokes drag to couple the particles and fluid and note that the Reynolds number is small in all simulations.

In addition to these recent numerical studies, several experimental studies have considered the effect of inertia on suspension rheology (Bagnold 1954; Savage & McKeown 1983; Hanes & Inman 1985; Prasad & Kytömaa 1995; Dijksmann

Downloaded from https://www.cambridge.org/core. Universidad Nacional de Mexico (UNAM), on 26 Apr 2018 at 19:08:51, subject to the Cambridge Core terms of use, available at https://www.cambridge.org/core/terms. https://doi.org/10.1017/jfm.2016.763

Downloaded from https://www.cambridge.org/core. Universidad Nacional de Mexico (UNAM), on 26 Apr 2018 at 19:08:51, subject to the Cambridge Core terms of use, available at https://www.cambridge.org/core/terms. https://doi.org/10.1017/jfm.2016.763

et al. 2010). However, there are important distinctions between the experimental and numerical studies that complicate the comparisons of the results. In simulations, the density of the particles can be specified to equal that of the fluid. In experimental work, the particle and fluid densities may be difficult to match over all experimental conditions because of the temperature dependence of the densities. As discussed by Acrivos, Fan & Mauri (1994), Fall *et al.* (2009) and Dijksmann *et al.* (2010) any subsequent settling or floating of the particles can have a significant effect on the stress measurements. In addition for studies involving flow inertia, a simple shear flow is difficult to achieve because of macroscale flow transitions that may occur as a result of the experimental design (Hunt *et al.* 2002).

For this study, the focus is on neutrally buoyant suspensions with inertia. In the 1950s, Bagnold conducted experiments using 1 mm wax particles in water (Re ranged 20 to 400 and ϕ from 0.13 to 0.62) and the same particles in a more viscous water–glycerol–ethanol mixture (Re from 2 to 15 for $\phi = 0.55$). From the experimental measurements, Bagnold concluded that the flow transitioned from a linear, 'macroviscous' regime in which the stresses varied linearly with shear rate to a nonlinear, inertial regime in which the stresses varied quadratically on the shear rate. The experimental measurements, however, were conducted in a smooth-walled concentric cylinder rheometer with a rotating outer cylinder, rotating end plates and stationary inner cylinder. As shown by Hunt *et al.* (2002), the gap Reynolds number associated with the rheometer design (here the Reynolds number is based on the speed of the rotating wall and the gap size of the annulus, $Re_b = \rho\omega r_o b/\mu$, where ω is the rotational speed, r_o is the outer cylinder radius and b is the shear gap width) ranged from 800 to 28 000; the height of the rheometer, H, was small relative to the gap, $H/b = 4.6$. Hence for many of the experiments, the Reynolds number was high enough that the flow was no longer a simple shear flow but contained counter-rotating vortices at the end walls that contributed substantially to the torque and stress measurements. Hunt *et al.* (2002) concluded that the variation in shear stresses from a linear regime to a nonlinear regime resulted from the development of the vortical structures and not from particle-to-particle collisions described by Bagnold.

Following Bagnold (1954), Savage & McKeown (1983) used neutrally buoyant 1 mm polystyrene spheres in a coaxial-cylindrical rheometer with a rotating inner cylinder. Because their experiments involved gap Reynolds numbers beyond the critical Reynolds number, their rheological measurements were strongly affected by the secondary flows that resulted from the centrifugal instability due to the rotation of the inner cylinder.

As Reynolds numbers are increased in a suspension flow, turbulent fluctuations may contribute to the momentum transport. A study by Gore & Crowe (1989) compiled experimental measurements of the change in turbulent fluctuations for multiphase flows (liquid–solid, gas–solid, gas–liquid and liquid–gas) relative to single-phase flows in pipes or free jets. Their analysis across 15 different data sets showed for flows in which the particle diameter was greater than 10 % of the turbulence length scale ($d/l_t \geqslant 0.1$, where l_t is the turbulence length scale), such as the size of the most energetic eddy, the turbulent intensity of the carrier phase was increased. They concluded that particles larger than the most energetic eddy do not follow the turbulent motions and the relative motion produces wakes that enhance the turbulence. For pipe flows, they used a turbulence length scale $l_t \approx 0.1D$, where D is the pipe diameter; hence, their criteria suggest that particles with diameters greater than 1 % of the pipe diameter enhance the turbulent fluctuations. Work by Tanaka & Eaton (2008) argues that the concentration, density ratio and Reynolds number are also

Downloaded from https://www.cambridge.org/core. Universidad Nacional de Mexico (UNAM), on 26 Apr 2018 at 19:08:51, subject to the Cambridge Core terms of use, available at https://www.cambridge.org/core/terms. https://doi.org/10.1017/jfm.2016.763

important in determining the augmentation or attenuation of the turbulent fluctuations. As a note, these studies did not include neutrally buoyant particles and the studies focused on low solid fractions.

Another interesting aspect of particulate flows is the appearance of fluid velocity fluctuations (i.e. Reynolds stresses) resulting from the presence of a dispersed phase and not from the instability of the flow resulting from inertia. Both particulate and bubbly flows have been found to exhibit large Reynolds-like stresses at low Reynolds numbers that increase with the particle volume fraction (Cartellier & Riviere 2001; Martinez-Mercado, Palacios-Morales & Zenit 2007; Mendez-Diaz *et al.* 2013). Since the origin of these fluctuations is different from that of single-phase turbulent flows, these flows are often called pseudo-turbulent. It has been shown that the velocity fluctuations are a result of the distribution of particles in space rather than due to the nature of the flow around the particles (Risso 2011). It is also important to point out that self-diffusion in particulate flows, a subject that has been widely studied (Breedveld *et al.* 1998), is closely related to these turbulent-like fluctuations. These particle-induced fluctuations and an enhanced diffusivity are expected to influence the transition to ordinary turbulence but this aspect has not been addressed in detail in the literature. It should be noted that finite-inertia suspensions, in particular wall-bounded flows, are not necessarily homogeneous; therefore their analysis and understanding are more complex. For instance, Verberg & Koch (2006) and Kulkarni & Morris (2008) have reported on the effects of an inhomogeneous shear rate within bounded flows.

Neutrally buoyant particles were considered by Matas, Morris & Guazzelli (2003) in their experimental study of the effects of particles on the critical Reynolds number for flow in a pipe. Their results, based on pressure fluctuations in the flow, showed that critical Reynolds number depends on both the ratio of the pipe diameter to the particle diameter (D/d) and on the solid fraction. For particles with $D/d \geqslant 65$, the critical Reynolds number increased for all solid fractions examined (up to $\phi = 0.35$) and was independent of particle size; this delay in turbulent transition results from the increase in effective viscosity caused by the suspended particles. For larger particles in which $D/d \leqslant 65$, the critical Reynolds number either increased or decreased. For the largest particles considered ($D/d \approx 10$), the critical Reynolds number dropped from approximately 2000 to 1000 at $\phi = 0.07$; the authors suggest that the presence of the particles caused the flow to transition at a lower Reynolds number. Beyond $\phi = 0.07$, the critical Reynolds number increased reaching approximately 2700 at $\phi = 0.35$.

The current study follows the work of Koos *et al.* (2012) and uses the same experimental facility, which is described in the next section. In that study, the authors showed that for the range of Reynolds numbers, solid fractions and particles tested (Re from 20 to 800; ϕ from 0.07 to 0.6; three different types of particles) the effective viscosity had little dependence on the Reynolds number. However, the magnitude of the effective viscosity was substantially larger than predicted by an Eilers or Krieger–Dougherty model. In most of the experiments, the rheometer walls were smooth and the authors found substantial slip along with the walls. Hence, that work included some additional measurements for one type of particle with roughened walls. The roughness resulted in a further increase in the effective viscosity, presumably due to the increased agitation of the particles; however, the variation in the effective viscosity with Reynolds number only showed a slight increase at the lowest solid fractions. The experiments in this paper focus on measurements with roughened walls and neutrally buoyant particles. This work expands the conditions considered in Koos *et al.* (2012) to include a wider range of Reynolds numbers (Re ranges from 2 to 1000); in addition, this work reconsiders some of the experimental data found in Koos *et al.* (2012).

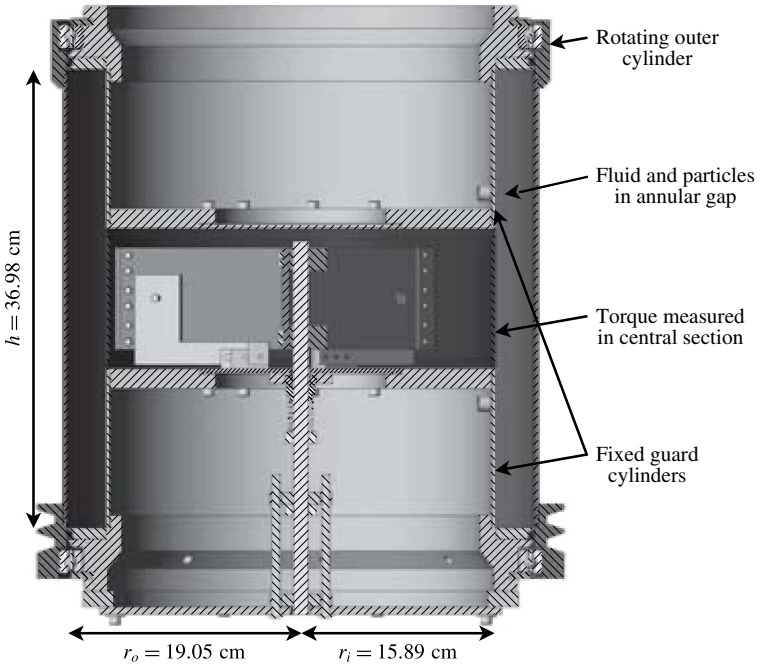

FIGURE 2. Schematic of the coaxial-cylinder rheometer.

2. Experimental rheometer and pure fluid studies

This study uses the coaxial-cylinder rheometer, as shown in figure 2 and described in detail by Koos *et al.* (2012). The inner cylinder is stationary and the outer cylinder is rotated by a belt connected to a motor; the maximum angular speed is $\omega = 15\ \mathrm{s}^{-1}$. To allow the torque measurements to be made in a region of the flow away from the corners where the flow is not a simple shear flow, the inner cylinder consists of three sections: the rigid top and bottom guard cylinders (each of height 12.7 cm) and a central, floating cylinder ($H = 11.22$ cm). The floating or test cylinder is supported by a central axle and its rotation is constrained by a calibrated spring to allow measurement of the torque or shear stress. To facilitate rotation, the cylinder is separated from the upper and lower guard cylinders by knife-edge gaps. The torque on the cylinder is computed from a measurement of the rotation of the central cylinder, the spring constant and the cylinder radius. The springs were calibrated prior to each experimental run. The spring calibration was done with the rheometer running to ensure similar experimental conditions. Springs with different stiffness are used to allow a range of torques (M) between $1.3 \times 10^{-3} \leqslant M \leqslant 2.7$ N m to be measured. In reviewing the data from Koos *et al.* (2012) it was noted that spring calibration was carried out just for pure fluid measurements; for the subsequent experiments with particles the torque measurements were constrained through the origin. Hence the analysis assumed that the relationship between torque and shear rate was linear. The slope of the linear fit was used by Koos *et al.* (2012) to find the effective viscosity of the mixture. Therefore, any error in the y-intercept in the flow curve (shear stress versus shear rate) can affect the value of the averaged shear stress. As a note, the intercept could have a non-zero value, similar to a yield stress, if the particles had settled because of a density mismatch between the fluid and the particles. In § 4, some of the data are reconsidered without the zeroing of the calibration.

Downloaded from https://www.cambridge.org/core. Universidad Nacional de Mexico (UNAM), on 26 Apr 2018 at 19:08:51, subject to the Cambridge Core terms of use, available at https://www.cambridge.org/core/terms. https://doi.org/10.1017/jfm.2016.763

Downloaded from https://www.cambridge.org/core. Universidad Nacional de Mexico (UNAM), on 26 Apr 2018 at 19:08:51, subject to the Cambridge Core terms of use, available at https://www.cambridge.org/core/terms. https://doi.org/10.1017/jfm.2016.763

The current experiments are conducted using polystyrene elliptical cylinders with major axis length 2.92 mm and minor axis length 2.08 mm; the particles have smooth walls but are rough cut with average length of 3.99 mm. An equivalent sphere diameter is 3.34 mm. These particles were also used in Koos *et al.* (2012) along with spheres and spheroids. Unlike the particle shape dependence found in low *Re* regime rheological measurements (Mallavajula, Kock & Archer 2013; Audus *et al.* 2015), the measurements from Koos *et al.* (2012) did not show a difference with particle geometry.

In Koos *et al.* (2012) the random loose-pack and close-pack volume fractions were reported as 0.553 and 0.663. In the current work the rheological measurements are performed with walls roughened, which involved gluing these same particles to thin sheets and then attaching the sheets to the inner and outer cylinders. Without roughness, the inner radius of the annulus, r_i, is 15.89 cm, the outer radius of the annulus, r_o, is 19.05 cm and the width of the annulus between the cylinders, b, is 3.16 cm. With roughness, these averaged dimensions are $r_i = 16.22$ cm, $r_o = 18.72$ cm, and $b = 2.49$ cm. Note that the device used in this investigation has a gap of approximately 7.5 particle diameters. Clearly, some local inhomogeneities are expected (as discussed by Koos *et al.* 2012), resulting from this finite gap size. To simplify the analysis, no attempt to correct for this effect was made, which would require a determination of the particle distribution within the gap. The density of the polystyrene particles is 1050 kg m^{-3}, which are the lowest-density particles used by Koos *et al.* (2012).

For the suspension experiments two different liquids were used. To match the density of the particles, the liquids were either a mixture of approximately 79 % water and 21 % glycerol (low-viscosity fluid) or a mixture of 58 % ethanol and 42 % glycerol (high-viscosity fluid). For each experiment, the fluid density and temperature were measured and used to determine the fluid viscosity. At 22 °C, the viscosity of the ethanol–glycerol mixture was 0.030 Pa s and 0.0018 Pa s for the glycerol–water mixture. The differences in densities between the particles and fluid were less than 1 %. Although the density differences were small, some settling or flotation of the particles could be observed due to temperature changes, which was similar to that observed in the experiments by Acrivos *et al.* (1994).

Prior to the suspension studies, tests with liquids without particles were run to test the experimental method. These measurements were conducted considering four different fluids. For all cases, both for the suspensions and pure liquid tests, each measurement was repeated at least five times. In this manner, the standard deviation of each experiment could be calculated to assess the uncertainty of the measurement. For each experimental condition (a combination of fluid and particle concentration), measurements were obtained by gradually increasing the angular speed of the set-up. In some cases, for the same nominal conditions, the experiments were repeated on different days and considering different springs to ensure repeatability of the results.

For a single-phase viscous fluid in annular shear flow with outer rotating wall, the torque, M_{lam}, is computed as

$$M_{lam} = 2\pi\mu\dot{\gamma}Hr_i^2, \tag{2.1}$$

where the shear rate, $\dot{\gamma}$, is computed from the rotational speed and annulus geometry, $\dot{\gamma} = 2\omega r_o^2/(r_o^2 - r_i^2)$. In Koos *et al.* (2012), pure fluid torque measurements were also conducted for a smooth-walled rheometer. Those measurements showed laminar behaviour up to $Re_b = 6000$; the torques were within 20 % of the laminar flow values

with the highest deviation occurring at the lowest shear rates. For flow between concentric cylinders with rotation of the inner cylinder, there is a complex set of transitions that depend on the Reynolds number of the inner cylinder and the geometry (see Taylor 1936*a*,*b*, Coles 1965, Swinney & Gollub 1978). However, for a flow in which only the outer cylinder rotates, the flow is 'azimuthal laminar flow with weak Ekman vortices' (Andereck, Liu & Swinney 1986) below a critical Reynolds number. The Ekman vortices arise because of the end walls; the strength of these vortices depends on the geometry and whether the end walls are fixed or rotate (Coles 1965; VanAtta 1966; Andereck *et al.* 1986). For a rotating outer cylinder, the early work by Taylor (1936*a*) and Wendt (1933) used torque measurements to determine the critical Reynolds number at which transition occurs for different radii of the inner and outer cylinders.

Of particular interest for the present study are the papers by Coles (1965) and VanAtta (1966), which also involved flow between rotating cylinders. Their work does not include torque measurements but does examine the transition from laminar to turbulent flow and includes Reynolds numbers over the range found in the current experiments (this range is larger than that found in Andereck *et al.* (1986)). They found that for flows with a rotating outer cylinder there was a range of Reynolds numbers in which the flow could be either laminar or turbulent depending on the process for starting the flow and on the height of the annular region relative to the gap. If the Reynolds number was beyond the critical value, the rotational speed had to be reduced to a fraction of the critical speed to return the flow to a laminar state.

In the more recent torque measurements by Ravelet, Delfos & Westerweel (2010), the laminar to turbulent transition is described as 'very sharp'. For these experiments, the height was considerably larger than the gap, $H/b = 22$. The critical Reynolds number found in the study of Ravelet *et al.* (2010) was approximately 4000 for $b/r_o = 0.083$, which is consistent with the critical Reynolds number based on Taylor's data. Ravelet *et al.* (2010) also measured the circumferential velocity distribution for supercritical speeds and found steep velocity gradients at the inner and outer walls and a flattened central region as compared with the laminar flow profile. With rotation of the outer wall (their end walls also rotated), they did not observe any large-scale turbulent structures within the flow.

For the smoothed-wall rheometer, the critical Reynolds number can be estimated based on the ratio of the gap width to outer radius ratio, b/r_o from the work by Taylor (1936*a*). For $b/r_o = 0.17$, the critical Reynolds number is estimated as $Re_c = 1.6 \times 10^4$. With rough walls, the gap width and outer radius are smaller ($b/r_o = 0.13$), which results in a lower critical Reynolds number of 1×10^4.

Figure 3 presents the measured torque for pure fluid, M, normalized by M_{lam} for the current work and the data from Taylor (1936*a*) and Ravelet *et al.* (2010); the data show a transition around $Re_b = 4 \times 10^3$, lower than the critical Reynolds number based on the work of Taylor (1936*a*). However, the current experiments involve rough-walled cylinders, which appear to cause a transition to turbulent flow at a lower Reynolds number. This finding contrasts with a study by Lee *et al.* (2009) using a rotating inner cylinder and stationary outer cylinder with axial slits; in that study the critical Reynolds number at which the laminar instability first occurred did not change although the transition to turbulence was accelerated.

As found in figure 3, one data set from Taylor (1936*a*) (for $b/r_o = 0.15$) shows a relatively smooth transition, while the second data set (for $b/r_o = 0.11$) shows a sharp transition in which the torque increases by a factor of 2. Although not shown, the experiments by Wendt (1933) also show a sharp transition (these data can also be found in the paper by Hunt *et al.* (2002)).

Downloaded from https://www.cambridge.org/core. Universidad Nacional de Mexico (UNAM), on 26 Apr 2018 at 19:08:51, subject to the Cambridge Core terms of use, available at https://www.cambridge.org/core/terms. https://doi.org/10.1017/jfm.2016.763

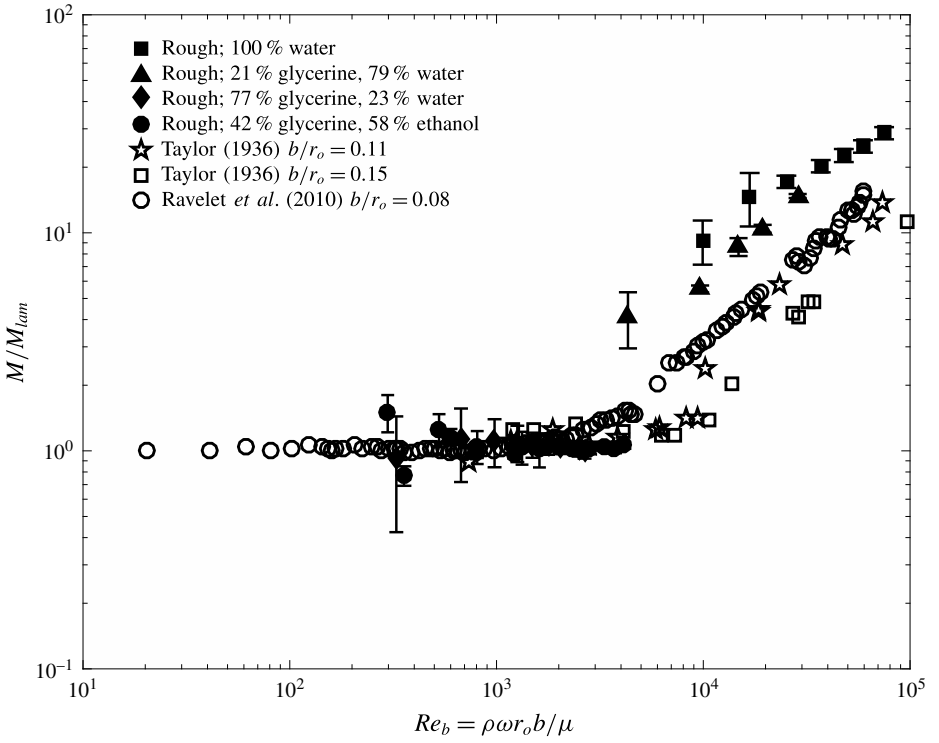

FIGURE 3. Measured torque normalized by the theoretical pure fluid torque considering laminar flow, as a function of gap Reynolds number for different fluids. Open symbols correspond to the data from Taylor (1936*a*) and Ravelet *et al.* (2010).

In addition, the recent experiments by Ravelet *et al.* (2010) also show a gradual increase in torque starting around $Re = 1000$ followed by a significant jump at $Re \approx 5000$. The variation in these measurements is probably a result in the differences in the height of the annulus relative to the gap size and the method of increasing or decreasing the rotational speed to arrive at the final state (Coles 1965; VanAtta 1966).

With regard to the current data, figure 3 shows that the normalized torque does not increase before $Re \approx 4000$. At this Reynolds number, the torque ratio shows a sharp increase. The difference between the current data and earlier studies involves the use of the central and guard cylinders; with this experimental design the torque measurements do not include the contributions from the end wall regions; instead the torque shows a sudden change in magnitude that corresponds with a fully turbulent flow. Beyond the critical Reynolds number, the normalized torque is greater than that found in the two sets of experiments by Taylor (1936*a*) for $b/r_o = 0.115$ and 0.148 and in the experiments from Ravelet *et al.* (2010) for $b/r_o = 0.083$. However, an increase in magnitude of torque because of wall roughness is consistent with the earlier studies in which the torque was measured for flow in an annulus with an inner rotating cylinder (Cadot *et al.* 1997; van den Berg *et al.* 2003) and with studies involving turbulent flow along a roughened plate or in a tube.

For flow between coaxial cylinders with either one or both cylinders rotating, the dimensionless torque is often expressed as

$$G = ARe_b^{\alpha} \tag{2.2}$$

Downloaded from https://www.cambridge.org/core. Universidad Nacional de Mexico (UNAM), on 26 Apr 2018 at 19:08:51, subject to the Cambridge Core terms of use, available at https://www.cambridge.org/core/terms. https://doi.org/10.1017/jfm.2016.763

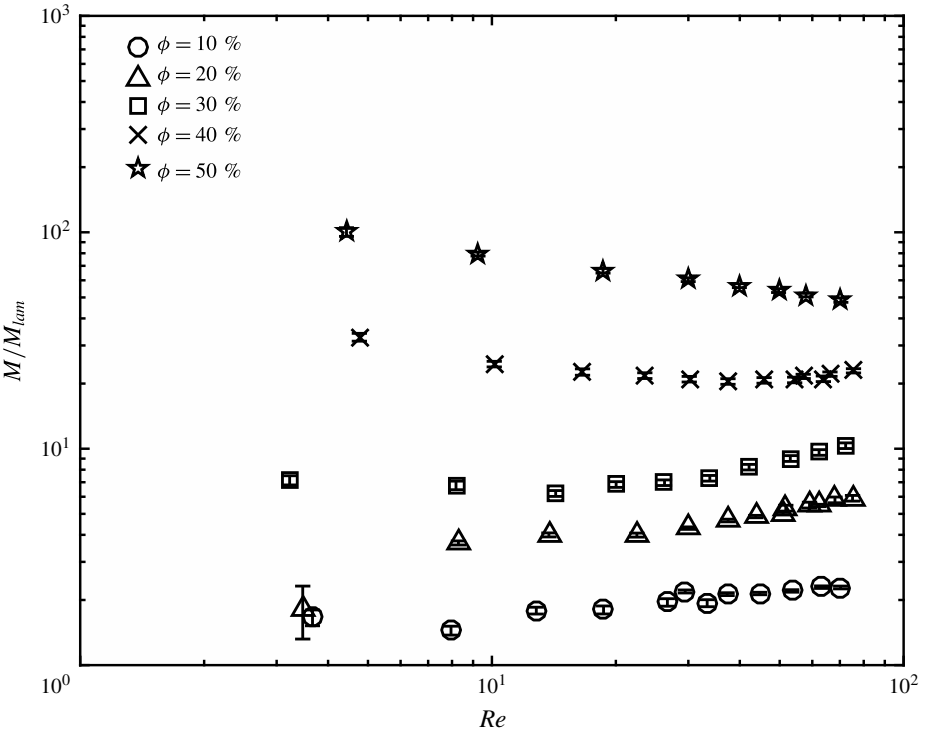

FIGURE 4. Measured torque normalized by the theoretical pure fluid torque considering laminar flow, as a function of Reynolds number for polystyrene particles immersed in a glycerol–ethanol solution (high-viscosity fluid).

where $G = T/(2\pi H\mu^2/\rho)$ and A is a constant. For laminar flow, the value of A is computed as $A = 2r_o r_i^2/[(r_o - r_i)^2(r_o + r_i)]$ and $\alpha = 1$. The current data for $Re_b > 4000$ are best represented using $\alpha \approx 1.7$. The study by Ravelet *et al.* (2010) for an outer rotating cylinder found α changes from 1 to approximately 1.75 as the Reynolds number increased from 1000 to 5000 with a critical Reynolds number of approximately 2000. In the work by van den Berg *et al.* (2003) for turbulent flow in Taylor–Couette flow with a rotating inner cylinder, they found that the value of the exponent α was equal to 2 when both walls were rough; for smooth walls, $\alpha = 1.67$, and for one smooth and one rough wall the value fell between $\alpha = 1.8$ and 1.9 for Reynolds numbers (based on the speed of the inner wall) up to 10^6.

3. Experiments with neutrally buoyant particles

Figure 4 presents the torque measurements normalized by the torque for laminar flow (M/M_{lam}) for the polystyrene particles in the glycerol–ethanol mixture for ϕ from 0.1 to 0.5. Figure 5 shows on a linear scale the same data for $\phi = 0.1$, 0.2, and 0.3 along with the simulations of Picano *et al.* (2013); the data from Kulkarni & Morris (2008) and from Yeo & Maxey (2013) are not shown because of the lower Reynolds numbers considered in those studies. For $\phi = 0.1$ the normalized torque, or equivalently the effective viscosity, is approximately constant for Re from 3 to approximately 18 and then increases for higher Reynolds numbers. As shown in figure 5, the experimental data for $\phi = 0.1$ compare well with the simulations from

Downloaded from https://www.cambridge.org/core. Universidad Nacional de Mexico (UNAM), on 26 Apr 2018 at 19:08:51, subject to the Cambridge Core terms of use, available at https://www.cambridge.org/core/terms. https://doi.org/10.1017/jfm.2016.763

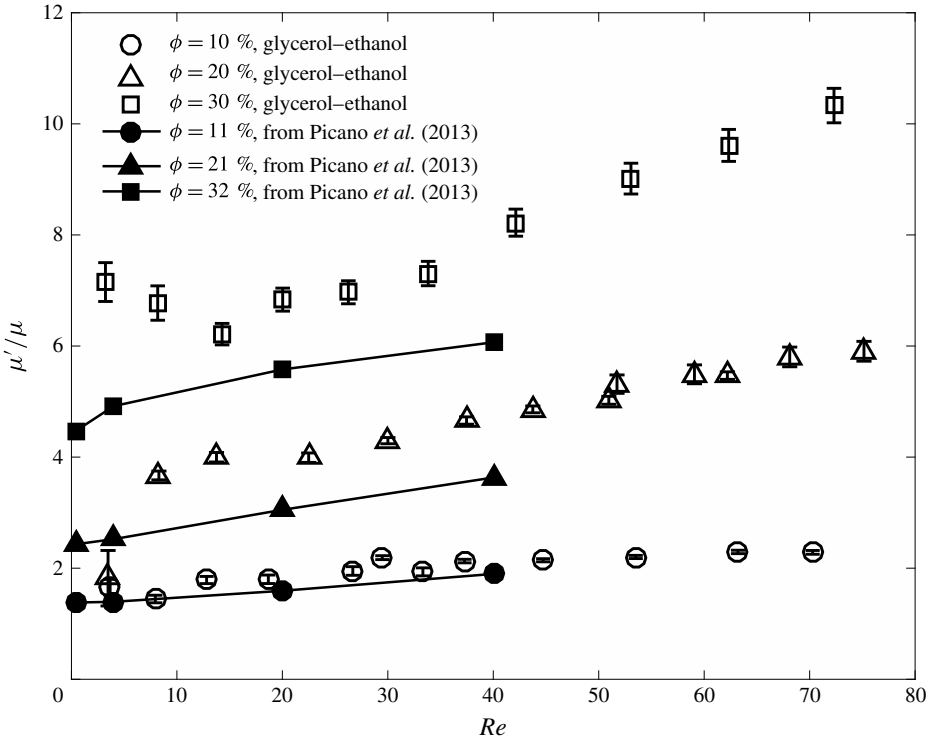

FIGURE 5. Normalized torque (experiments) and effective viscosity (numerical results) as a function of Reynolds number. The experiments correspond to the polystyrene particles immersed in a high-viscosity fluid for $\phi = 0.1$, 0.2 and 0.3. The simulations results are from Picano *et al.* (2013).

Picano *et al.* (2013). For $\phi = 0.2$, the normalized torques increase over the range of Reynolds numbers examined. Except for the experimental data point at $Re = 2.5$, the experimental measurements are approximately 40 % higher than the values from the Picano *et al.* (2013) simulations. For $\phi = 0.3$, the experimental measurements show a slight shear thinning for $Re < 10$ followed by a subsequent increase for Re from 15 to 60. At $Re = 40$, the experimental measurements are approximately 50 % higher than the simulations. Possible reasons for the differences are discussed in the next section.

For the highest solid fractions, $\phi = 0.4$ and $\phi = 0.5$, the normalized torques are found in figure 4 and are distinct from the behaviour found at lower solid fractions. For $\phi = 0.4$, the normalized torque shows a shear thinning behaviour until approximately $Re = 20$, followed by shear thickening. For $\phi = 0.5$, the normalized torque decreases over the entire range of Reynolds numbers.

Figure 6 shows the measurements of the normalized torque (M/M_{lam}) for the same particles in the glycerol–water mixture resulting in Reynolds numbers greater than 100. For $\phi = 0.1$, 0.2 and 0.3, the normalized torques increase with Reynolds number. For $\phi = 0.4$ and $\phi = 0.5$, the normalized torques show little variation with Reynolds number.

Figure 7 shows both sets of data for $\phi = 0.1$, 0.2, and 0.3 as a function of the gap Reynolds number, Re_b. The results using the glycerol–water mixture have

Downloaded from https://www.cambridge.org/core. Universidad Nacional de Mexico (UNAM), on 26 Apr 2018 at 19:08:51, subject to the Cambridge Core terms of use, available at https://www.cambridge.org/core/terms. https://doi.org/10.1017/jfm.2016.763

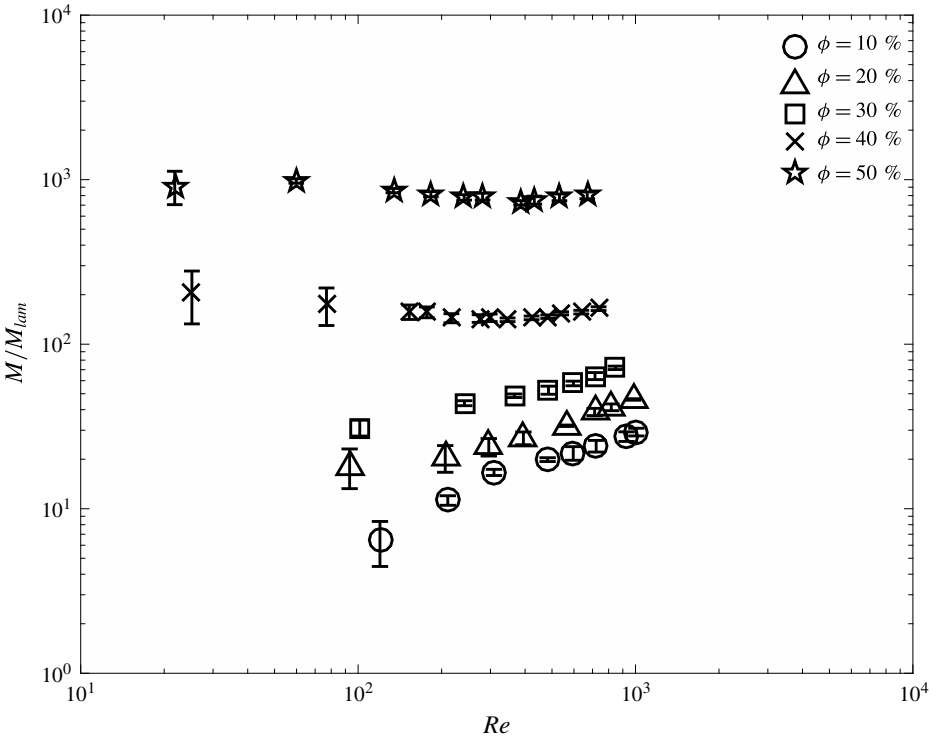

FIGURE 6. Normalized torque as a function of Reynolds number for polystyrene particles immersed in the glycerol–water solution (low-viscosity fluid).

torques that are higher than might be anticipated if the torques measured using the glycerol–ethanol mixture are extrapolated to higher Reynolds numbers. As a note the rheometer was run over its full range of speeds; unfortunately, there is no overlap in Reynolds numbers between the two data sets. Also shown in the figure are the measurements for the glycerol–water mixture without particles; these points are correlated by $M(\phi = 0)/M_{lam} = 0.0123 Re_b^{0.68}$. As mentioned in the context of figure 3, the pure fluid measurements are found to have transitioned to turbulent flow. The glycerol–water data for $\phi = 0.1$ parallel the data set for the pure fluid; the data for $\phi = 0.2$ and 0.3 also follow the pure fluid curve although the dependence on Reynolds number is not as strong. Like the pure fluid measurements, the glycerol–water data appear to have transitioned to a turbulent flow; the sharp transition is a result of the experimental design. Although not shown, the dimensionless torque measurements for the glycerol–ethanol mixture without particles was approximately $M/M_{lam} = 1$ up to $Re_b = 4000$.

Figure 8 presents the torque measurements M/M_{lam} for both data sets for $\phi = 0.1$, 0.2, and 0.3; however, with the purpose of separating the effect of solid fraction, the viscosity used in calculating M_{lam} and Re_b is obtained considering the Krieger–Dougherty relation $\mu' = \mu(1 - \phi/\phi_m)^{-1.82}$ and using $\phi_m = 0.58$. That is,

$$Re_b' = \frac{\rho \omega r_o b}{\mu(1 - \phi/\phi_m)^{-1.82}} \tag{3.1}$$

$$M_{lam}' = 2\pi\mu(1 - \phi/\phi_m)^{-1.82}\dot{\gamma} H r_i^2. \tag{3.2}$$

Downloaded from https://www.cambridge.org/core. Universidad Nacional de Mexico (UNAM), on 26 Apr 2018 at 19:08:51, subject to the Cambridge Core terms of use, available at https://www.cambridge.org/core/terms. https://doi.org/10.1017/jfm.2016.763

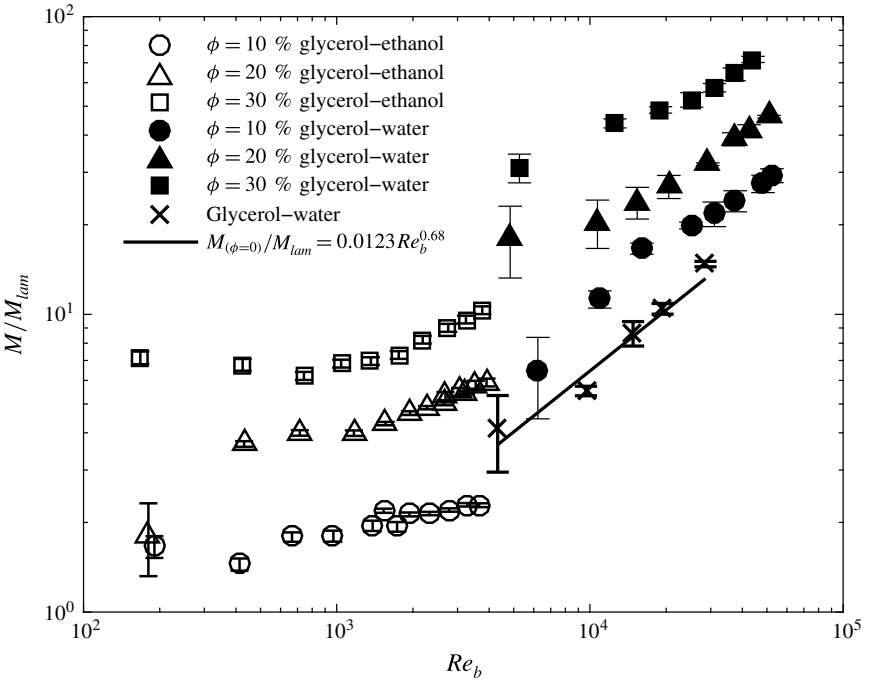

FIGURE 7. Normalized torque as a function of gap Reynolds number for polystyrene particles immersed in the high- and low-viscosity fluids, respectively.

This expression was also used by Matas *et al.* (2003) for transitional flows with particle Reynolds numbers beyond 10. Also, shown by the dotted line, is the best fit to the single-phase flow measurements. Note that, as found in figure 2, the pure fluid data show a transition to turbulent flow at $Re_b \approx 4000$. For the measurements with particles, the data suggest a similar flow transition around $Re_b' \approx 3000$; however, the critical Reynolds number shows dependence on solid fraction with the higher solid fractions transitioning at slightly lower Reynolds numbers. This variation in the critical Reynolds number with solid fraction is similar to that seen by Matas *et al.* (2003) for flow in a pipe with relatively large particles.

Figure 9 shows the normalized torque measured for the glycerol–water experiments along with some data from the work by Koos *et al.* (2012) involving the rough-walled rheometer. As noted earlier, the normalized torques from Koos *et al.* (2012) rough-walled experiments were independent of Reynolds number. However in reconsidering the data calibration as described in § 2, the normalized torque measurements for the lowest solid fractions do show a variation with Reynolds number as found in figure 9. For the lowest solid fractions, the Koos *et al.* (2012) torque measurements are lower than in the current data. Moreover, the earlier data for $\phi = 0.1$ are lower than the torque measurements for a pure fluid. This difference in magnitude is probably due to the difference in roughness between the 2012 measurements and the current data set. In 2012, the roughness was created by pressing and gluing the particles into a 1 mm rubber sheet, which created a less rough surface compared with the current experiments that used a thinner (0.15 mm) sheet. Hence the torque measurements are affected by the extent of the roughness of the surface.

Downloaded from https://www.cambridge.org/core. Universidad Nacional de Mexico (UNAM), on 26 Apr 2018 at 19:08:51, subject to the Cambridge Core terms of use, available at https://www.cambridge.org/core/terms. https://doi.org/10.1017/jfm.2016.763

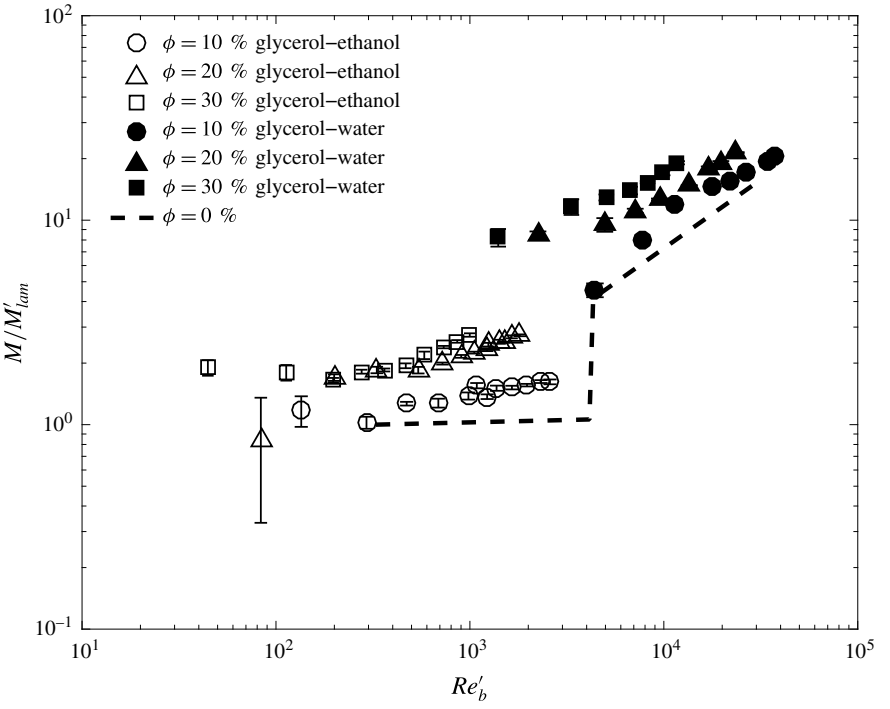

FIGURE 8. Measured torque normalized by effective laminar torque (using the effective viscosity from the Krieger–Dougherty relation) as a function of effective gap Reynolds number for polystyrene particles immersed in the high- and low-viscosity fluids, respectively.

In figure 10, the torque measurements for all of the experiments are presented using the normalization $G' = M/(H\mu'^2/\rho)$ as a function of Re'_b using the Krieger–Dougherty model for μ' based on the form used in Matas *et al.* (2003). The solid and dashed lines are the results for a pure fluid. As noted in the context of (2.2), the magnitude of G' depends linearly on Re'_b for laminar flow and was found to depend on $Re_b^{1.7}$ for the pure-fluid experiments beyond the critical Reynolds number. As shown in the figure, the data using glycerol–ethanol (high-viscosity fluid) for the lowest values of Re'_b and for all solid fractions follow the laminar flow result; however, the slopes for the highest solid fractions are shallower than that for laminar flow. Around Re'_b of 500, the data begin to deviate from the laminar flow result and show a higher dependence on the Reynolds number. For the experiments using glycerol–water (low-viscosity fluid) for $\phi = 0.1$, the experimental results closely match the results for a pure fluid. For $\phi = 0.2$ and 0.3 the results show a weaker dependence on Re'_b as compared with the pure fluid; an effective viscosity model is also less appropriate for predicting the experimental data. For $\phi = 0.4$ and 0.5, the normalized torques G' have a weaker dependence on Reynolds number. The data also show a difference in the magnitude of the normalized torques between the results for glycerol–ethanol and the glycerol–water mixtures; possible reasons for the differences are given in the next section. Note that the two parameters used in the Krieger–Dougherty model (the value of ϕ_m and the exponent) can be varied to provide a better collapse of the high-viscosity data at the lowest values of Re'_b. However, modifications to the Krieger–Dougherty parameters do not simultaneously provide a collapse of the low-viscosity measurements.

Downloaded from https://www.cambridge.org/core. Universidad Nacional de Mexico (UNAM), on 26 Apr 2018 at 19:08:51, subject to the Cambridge Core terms of use, available at https://www.cambridge.org/core/terms.
https://doi.org/10.1017/jfm.2016.763

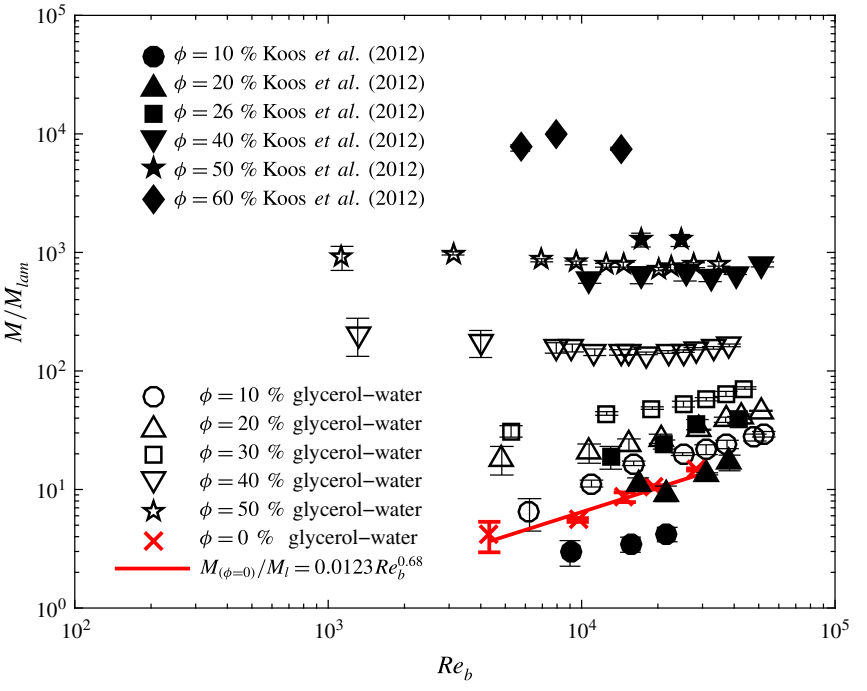

FIGURE 9. (Colour online) Comparison between the normalized torques for the low-viscosity fluid and the results from Koos *et al.* (2012) for rough-walled experiments.

4. Discussion and conclusion

For neutrally buoyant suspension of particles in which $Re > 1$, the bulk stress increases with Reynolds number due to the inertia of the particles and the fluid (Batchelor 1970). The presence of the particles also results in velocity fluctuations that enhance the transport (Cartellier & Riviere 2001; Martinez-Mercado *et al.* 2007; Mendez-Diaz *et al.* 2013). As the Reynolds number is increased further, the inertia of the flow may cause a transition to turbulence. Prior studies have suggested that the particle may either enhance or suppress the turbulence (Gore & Crowe 1989; Matas *et al.* 2003). In addition if the particle Stokes number is greater than 10, collisions between particles or with a bounding surface may also increase the bulk stress (Joseph *et al.* 2001).

In the current experiments, the measured torque is used to compute the effective viscosity. For $Re < 100$ and $\phi = 0.10$, the effective viscosity shows an increase with Reynolds number, which is comparable with recent numerical simulations (Kulkarni & Morris 2008; Picano *et al.* 2013; Yeo & Maxey 2013). According to Kulkarni & Morris (2008), the increase results from the inertial effects on the calculation of the stresslet and is not due to the particle or velocity fluctuations. For $\phi = 0.2$ and for $\phi = 0.3$ for $10 < Re < 100$, the effective viscosity in the experiments also increases with Reynolds but at a rate that is higher than the numerical simulations. Because the experiments do not include detailed measurements of the particle or fluid velocities, it is not possible to conclude the reason for the difference. One possibility, however, may involve the roughness along the side walls, which reduces slip along the side walls and increases the particle velocity fluctuations (Koos *et al.* 2012). As previously noted the simulations were either for a simple shear flow or for a bounded flow using

Downloaded from https://www.cambridge.org/core. Universidad Nacional de Mexico (UNAM), on 26 Apr 2018 at 19:08:51, subject to the Cambridge Core terms of use, available at https://www.cambridge.org/core/terms. https://doi.org/10.1017/jfm.2016.763

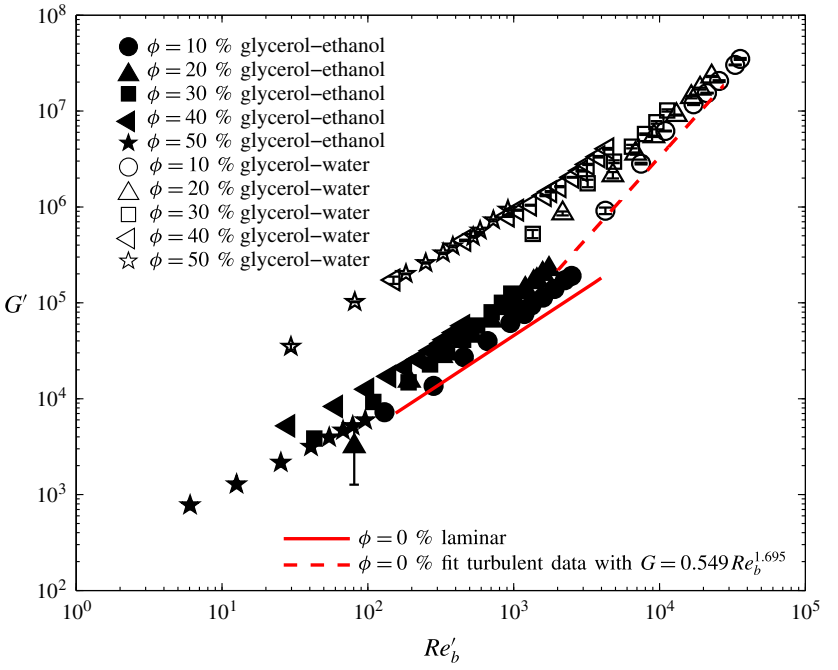

FIGURE 10. (Colour online) Normalized torque measurements for all of the current experimental measurements, G' as a function of Re'_b using an effective viscosity model.

smooth walls; the wall-bounded simulations showed considerable wall slip, especially for the higher solid fractions (Kulkarni & Morris 2008; Picano *et al.* 2013). Hence, the roughness may increase the velocity fluctuations of both the fluid and solid phases resulting in an increase in the Reynolds stresses beyond that calculated in the numerical studies. For $Re < 10$, the Stokes numbers are less than 10 so that particle collisions are not expected to contribute to the stresses. Within the corresponding range of Re_b, the pure fluid results are laminar.

For higher values of Re_b, the pure fluid experiments show a transition to turbulence as shown in figure 8; the results for the corresponding experiments with particles also show a transition. For $Re > 100$ and for $\phi < 0.30$, the effective viscosities show an increased dependence on the Reynolds number as compared with the results for the lower Reynolds numbers. In terms of the critical Reynolds number, the results show a slight decrease as the solid fraction is increased from $\phi = 0.1$ to 0.3. Hence, the particles not only increase the effective viscosity but also increase the fluid velocity fluctuations and promote turbulence. In addition, the torque and shear stresses are also affected by the wall roughness as found in the comparison with the data from Koos *et al.* (2012).

In looking at all of the data, as found in figure 10, the experiments for the high-viscosity fluid can be modelled using a modified version of the Krieger–Dougherty effective viscosity model. When presented in this form, there is a transition beginning around $Re'_b = 500$ to a higher dependence on Re that extends from the high-viscosity to the low-viscosity data. Although the results for ϕ=0.10 are well predicted using the turbulent result with an effective viscosity, the data for the higher solid fractions show a weaker dependence on Reynolds number. Hence the enhancement of the velocity fluctuations may not be as strong as the solid fraction is increased.

Downloaded from https://www.cambridge.org/core. Universidad Nacional de Mexico (UNAM), on 26 Apr 2018 at 19:08:51, subject to the Cambridge Core terms of use, available at https://www.cambridge.org/core/terms. https://doi.org/10.1017/jfm.2016.763

The non-dimensional torque data $\phi = 0.4$ and 0.5 for the low-viscosity fluid show a roughly linear dependence on the Reynolds number, similar to that for a laminar flow. However, the magnitude of the torques is significantly larger, and larger than predicted using the Krieger–Dougherty effective viscosity model. Earlier studies at high solid fractions suggest a change in the microstructure that shows a layering of the particles within the flow (Kulkarni & Morris 2008; Yeo & Maxey 2013). Although these studies were done at lower Reynolds numbers, similar changes in the microstructure may develop, especially for small gap size. Moreover, the differences between normalized torque for same high volume fraction but different interstitial liquid might be due to an increase in effective volume fraction due to settling, especially for the low-viscosity fluid. At the highest concentrations, a slight increase in volume fraction can result in a higher effective viscosity and a significantly lower value of G'.

Because the corresponding Stokes numbers for the glycerol–water experiments are from $St = 10$ to $St = 120$, particle collisions may also contribute to the stresses. Within this range of Stokes numbers, the coefficient of restitution increases from 0 to approximately 0.8 (Joseph *et al.* 2001; Yang & Hunt 2006). Hence, particle collisions may increase the stress transmission, especially for the higher Stokes number and more dilute flows.

It is important to note that all of the experiments were conducted for a single value of $b/d \approx 8$. Hence, future experiment should be performed for a range of particle sizes. In addition it would be useful to measure the velocity fluctuations and determine the microstructure of the flow to understand how the flow transitions as the solid fraction and Reynolds number increase.

Acknowledgements

We thank Professor C. E. Brennen for his comments and fruitful discussions. R.Z. is grateful to the Fulbright-Garcia Robles foundation and to the PASPA-DGAPA-UNAM program for their financial support during his sabbatical year at Caltech.

REFERENCES

ACRIVOS, A., FAN, X. & MAURI, R. 1994 On the measurements of the relative viscosity of suspensions. *J. Rheol.* **38** (5), 1285–1296.

ANDERECK, D., LIU, S. S. & SWINNEY, H. L. 1986 Flow regimes in a circular couette system with independently rotating cylinders. *J. Fluid Mech.* **164**, 155–183.

AUDUS, D. J., HASSAN, A. M., GARBOCZI, E. J. & DOUGLAS, J. F. 2015 Interplay of particle shape and suspension properties: a study of cube like particles. *Soft Matt.* **11**, 3360–3366.

BAGNOLD, R. A. 1954 Experiments on a gravity-free dispersion of large solid spheres in a Newtonian fluid under shear. *Proc. R. Soc. Lond.* A **225** (1160), 49–53.

BATCHELOR, G. K. 1970 The stress system in a suspension of force-free particles. *J. Fluid Mech.* **41**, 545–570.

VAN DEN BERG, T. H., DOERING, C. R., LOHSE, D. & LATHROP, D. 2003 Smooth and rough boundaries in turbulent Taylor–Couette flow. *Phys. Rev.* E **68**, 036307.

BREEDVELD, V., ENDE, D., VAN DEN TRIPATHI, A. & ACRIVOS, A. 1998 The measurement of the shear-induced particle and fluid tracer diffusivities in concentrated suspensions by a novel method. *J. Fluid Mech.* **375**, 297–318.

BREUGEM, W. P. 2012 A second-order accurate immersed boundary method for fully resolved simulations of particle-laden flows. *J. Comput. Phys.* **231** (13), 4469–4498.

BROWN, E., FORMAN, N. A., ORELLANA, C. S., ZHANG, H., MAYNOR, B. W., BETTS, D. E., DESIMONE, J. M. & JAEGER, H. M. 2010 Generality of shear thickening in dense suspensions. *Nat. Mater.* **9**, 220–224.

Downloaded from https://www.cambridge.org/core. Universidad Nacional de Mexico (UNAM), on 26 Apr 2018 at 19:08:51, subject to the Cambridge Core terms of use, available at https://www.cambridge.org/core/terms. https://doi.org/10.1017/jfm.2016.763

CADOT, O., COUDER, Y., DAERR, A., DOUADY, S. & TSINOBER, A. 1997 Energy injection in closed turbulent flows: stirring through boundary layers versus inerial stirring. *Phys. Rev.* E **56**, 427–433.

CARTELLIER, A. & RIVIERE, N. 2001 Bubble-induced agitation and microstructure in uniform bubbly flows at small to moderate particle Reynolds numbers. *Phys. Fluids* **13**, 2165–2181.

COLES, D. 1965 Transition in circular Couette flow. *J. Fluid Mech.* **21**, 385–424.

DIJKSMANN, J. A., WANDERSMANN, E., SLOTTERBACK, S., BERARDI, C. R., UPDEGRAFF, W. D., VAN HECKE, M. & LOSERT, W. 2010 From frictional to viscous behavior: three-dimensional imaging and rheology of gravitational suspensions. *Phys. Rev.* E **82**, 60301.

FALL, A., BERTRAND, F., OVARLEZ, G. & BONN, D. 2009 Yield stress and shear banding in granular suspensions. *Phys. Rev. Lett.* **103**, 178301.

FOSS, D. R. & BRADY, J. F. 2000 Structure, diffusion and rheology of Brownian suspensions by stokesian dynamics simulation. *J. Fluid Mech.* **407**, 167–200.

GORE, R. A. & CROWE, C. T. 1989 Effect of particle size on modulating turbulent intensity. *Intl J. Multiphase Flow* **15** (2), 279–285.

HANES, D. M. & INMAN, D. L. 1985 Observations of rapidly flowing granular-fluid materials. *J. Fluid Mech.* **150**, 357–380.

HUNT, M. L., ZENIT, R., CAMPBELL, C. S. & BRENNEN, C. E. 2002 Revisiting the 1954 suspension experiments of R. A. Bagnold. *J. Fluid Mech.* **452**, 1–24.

JOSEPH, G. G., ZENIT, R., HUNT, M. L. & ROSENWINKEL, A. M. 2001 Particle-wall collisions in a viscous fluid. *J. Fluid Mech.* **433**, 329–346.

KOOS, E., LINARES-GUERRERO, E., HUNT, M. L. & BRENNEN, C. E. 2012 Rheological measurements of large particles in high shear rate flows. *Phys. Fluids* **24**, 013302.

KULKARNI, P. M. & MORRIS, J. F. 2008 Suspension properties at finite Reynolds number from simulated shear flow. *Phys. Fluids* **20**, 40602.

LARSON, R. G. 1998 *Structure and Rheology of Complex Fluids*. Oxford University Press.

LEE, S. H., CHUNG, H. T., PARK, C. W. & KIM, H. B. 2009 Experimental investigation of the effect of axial wall slits on Taylor–Couette flow. *Fluid Dyn. Res.* **41**, 045502.

MALLAVAJULA, R. K., KOCK, D. L. & ARCHER, L. A. 2013 Intrinsic viscosity of a suspension of cubes. *Phys. Rev.* E **88**, 052302.

MARTINEZ-MERCADO, J., PALACIOS-MORALES, C. A. & ZENIT, R. 2007 Measurement of pseudoturbulence intensity in monodispersed bubbly liquids for $10 < Re < 500$. *Phys. Fluids* **19**, 103302.

MATAS, J. P., MORRIS, J. F. & GUAZZELLI, É. 2003 Transition to turbulence in particulate pipe flow. *Phys. Rev. Lett.* **90** (1), 4501–4504.

MENDEZ-DIAZ, S., SERRANO-GARCIA, J. C., ZENIT, R. & HERNANDEZ-CORDERO, J. A. 2013 Power spectral distributions of pseudo-turbulent bubbly flows. *Phys. Fluids* **25**, 043303.

PICANO, F., BREUGEM, W.-P. & BRANDT, L. 2015 Turbulent channel flow of dense suspensions of neutrally buoyant spheres. *J. Fluid Mech.* **764**, 463–487.

PICANO, F., BREUGEM, W. P., MITRA, D. & BRANDT, L. 2013 Shear thickening in non-Newtonian suspensions: an excluded volume effect. *Phys. Rev. Lett.* **111**, 098302.

PRASAD, D. & KYTÖMAA, H. K. 1995 Particle stress and viscous compaction during shear of dense suspensions. *Intl J. Multiphase Flow* **21** (5), 775–785.

RAVELET, F., DELFOS, R. & WESTERWEEL, J. 2010 Influence of global rotation and reynolds number on the large-scale features of a turbulent Taylor–Couette flow. *Phys. Fluids* **22**, 055103.

RISSO, F. 2011 Theoretical model for k3 spectra in dispersed multiphase flows. *Phys. Fluids* **23**, 011701.

SAVAGE, S. B. & MCKEOWN, S. 1983 Shear stresses developed during rapid shear of concentrated suspensions of large spherical particles between concentric cylinders. *J. Fluid Mech.* **127**, 453–472.

STICKEL, J. J. & POWELL, R. L. 2005 Fluid mechanics and rheology of dense suspensions. *Annu. Rev. Fluid Mech.* **37** (1), 129–149.

SWINNEY, H. L. & GOLLUB, J. P. 1978 The transition to turbulence. *Phys. Today* **31** (8), 41–49.

Downloaded from https://www.cambridge.org/core. Universidad Nacional de Mexico (UNAM), on 26 Apr 2018 at 19:08:51, subject to the Cambridge Core terms of use, available at https://www.cambridge.org/core/terms. https://doi.org/10.1017/jfm.2016.763

TANAKA, T. & EATON, J. K. 2008 Classification of turbulence modification by dispersed spheres using a novel dimensionless number. *Phys. Rev. Lett.* **101**, 114502.

TAYLOR, G. I. 1936*a* Fluid friction between rotating cylinders, I. Torque measurements. *Proc. R. Soc. Lond.* A **157** (892), 546–564.

TAYLOR, G. I. 1936*b* Fluid friction between rotating cylinders, II. Distribution of velocity between concentric cylinders when outer one is rotating and inner one is at rest. *Proc. R. Soc. Lond.* A **157** (892), 565–578.

TRULSSON, M., ANDREOTTI, B. & CLAUDIN, P. 2012 Transition from the viscous to inertial regime in dense suspensions. *Phys. Rev. Lett.* **109**, 118305.

VANATTA, C. 1966 Exploratory measurements in spiral turbulence. *J. Fluid Mech.* **25**, 495–512.

VERBERG, R. & KOCH, D. 2006 Rheology of particle suspensions with low to moderate fluid inertia at finite particle inertia. *Phys. Fluids* **18**, 083303.

WENDT, F. 1933 Turbulente strömungen zwischen zwei rotierenden konaxialen zylindern. *Ing.-Arch.* **4**, 577–595.

YANG, F. L. & HUNT, M. L. 2006 Dynamics of particle-particle collisions in a viscous liquid. *Phys. Fluids* **18**, 121506.

YEO, K. & MAXEY, M. R. 2013 Dynamics and rheology of concentrated, finite-Reynolds-number suspensions in a homogeneous shear flow. *Phys. Fluids* **25**, 533303.

Downloaded from https://www.cambridge.org/core. Universidad Nacional de Mexico (UNAM), on 26 Apr 2018 at 19:08:51, subject to the Cambridge Core terms of use, available at https://www.cambridge.org/core/terms. https://doi.org/10.1017/jfm.2016.763